

# Density functional theory study of the energetics, electronic structure, and core-level shifts of NO adsorption on the Pt(111) surface

Zhen-Hua Zeng,<sup>1,2</sup> Juarez L. F. Da Silva,<sup>3,\*</sup> Hui-Qiu Deng,<sup>4</sup> and Wei-Xue Li<sup>1,\*</sup>

<sup>1</sup>State Key Laboratory of Catalysis, and Center for Theoretical and Computational Chemistry, Dalian Institute of Chemical Physics, Chinese Academy of Sciences, Dalian 116023, China

<sup>2</sup>Graduate School of the Chinese Academy of Sciences, Beijing 100039, China

<sup>3</sup>National Renewable Energy Laboratory, 1617 Cole Boulevard, Golden, Colorado 80401, USA

<sup>4</sup>Department of Applied Physics, Hunan University, Changsha 410082, China

(Received 13 February 2009; revised manuscript received 9 April 2009; published 18 May 2009)

In this work, we report a first-principles investigation of the energetics, structures, electronic properties, and core-level shifts of NO adsorption on the Pt(111) surface. Our calculations are based on density functional theory within the framework of the ultrasoft pseudopotential plane-wave and the all-electron projected augmented-wave methods. We found that at 0.25, 0.50, and 0.75 monolayer, NO adsorbs preferentially in the fcc, fcc+top, and fcc+top+hcp sites, respectively. The geometric parameters, adsorption energies, vibrational frequencies, and work-function changes are in good agreement with the experimental data. The interaction between NO and Pt(111) was found to follow a donation–back-donation process, in which the NO  $\sigma$  states donate electrons to the substrate Pt  $d$  states, while the substrate Pt  $d$  states back donate to the NO  $\pi$  states. Though there is an overall net charge transfer from the substrate to the NO adsorbate regardless of the adsorption sites and coverages, the spatial redistribution of the transferred electron is site dependent. The charge accumulation for NO in the top sites occurs closer to the surface than NO in the hollow sites, which results in the reduction of the Pt(111) surface work function for the top NO but an increase for the hollow NO. The core-level shifts of the topmost surface Pt atoms coordinated with top and hollow NO molecules at different coverages are in excellent agreement with experiments. In contrast, the N  $1s$  core-level shifts between top and hollow NO ( $\sim 0.7$  eV) deviated significantly from the zero shift found in experiments. Our analysis indicates that the difference may come from the thermal vibration and rotation of adsorbed NO on the Pt(111) surface.

DOI: [10.1103/PhysRevB.79.205413](https://doi.org/10.1103/PhysRevB.79.205413)

PACS number(s): 68.43.Bc, 68.43.Fg, 79.60.-i

## I. INTRODUCTION

Transition-metal (TM) particles of Pt, Pd, and Rh supported on oxide surfaces are some of the main components of automotive three-way-catalyst devices, which are used to decrease pollutants from combustion exhausts.<sup>1</sup> Among them, carbon monoxide (CO), partially burned hydrocarbons, nitrogen oxides (NO<sub>x</sub>), and mostly NO are considered the most common pollutants (see Ref. 2 and references therein). The identification of the bonding strength and adsorption site preferences of the mentioned molecular species on TM surfaces is crucial in obtaining an atom-level picture of catalytic activities. The adsorption of NO on the Pt(111) surface has been widely addressed in experimental<sup>3–10</sup> and theoretical studies,<sup>11–17</sup> however, even for this apparent “simple” and well-defined system, several questions remain open and in debate. In this work, we will report a systematic investigation of the adsorption of NO on the Pt(111) surface employing first-principles calculations.

The adsorption of NO on Pt(111) has been characterized experimentally by low-energy electron diffraction (LEED),<sup>3,4</sup> dynamical LEED-IV,<sup>8</sup> scanning tunneling microscopy (STM),<sup>6,7</sup> high-resolution electron energy-loss spectroscopy (HREELS),<sup>7</sup> near-edge x-ray absorption fine spectroscopy (NEXAFS),<sup>5,10</sup> and temperature programmed x-ray photoelectron spectroscopy (XPS).<sup>9</sup> These studies found that adsorbed NO forms commensurate (2×2) structures on Pt(111) at coverages ( $\Theta_{\text{NO}}$ ) of 0.25, 0.50, and 0.75 monolayer (ML), which are stable up to about 320, 275, and 190

K, respectively.<sup>9</sup> For  $0 \leq \Theta_{\text{NO}} \leq 0.25$  ML, NO is found to adsorb preferentially at the threefold fcc sites, noted as (2×2)-NO(fcc), and there are no evidences for the occupation of the top sites. First-principles calculations<sup>12</sup> obtained that the fcc and hcp sites differ slightly in energy, while the top site is rather unfavorable. Thus, one would expect that the hcp site would be occupied by NO for coverages larger than 0.25 ML. However, no experiments confirmed this so far. Instead, NO adsorption in the top site was found. For example, for  $\Theta_{\text{NO}} > 0.25$  ML, NO populates gradually the top sites and forms the (2×2)-2NO(fcc+top) structure at  $\Theta_{\text{NO}} = 0.50$  ML. For  $\Theta_{\text{NO}} > 0.50$  ML, NO adsorbs to the hcp sites and forms the (2×2)-3NO(fcc+top+hcp) structure at 0.75 ML. The structure models, namely, (2×2)-NO(fcc), (2×2)-2NO(fcc+top), and (2×2)-3NO(fcc+top+hcp), are supported by the first-principles calculations.<sup>11–17</sup> We want to point out that the mechanism that drives the occupation of the top sites by NO at coverages higher than 0.25 ML remains unclear. Aizawa *et al.*<sup>12</sup> suggested that the relaxations of the topmost Pt(111) layers determine the stability of the fcc+top structure at 0.50 ML, however, only modest variation of the interlayer spacing induced by NO adsorption (about 1% to 3%) was reported in that work.

Recently, Zhu *et al.*<sup>9</sup> studied the adsorption of NO on Pt(111) using XPS and the core-level shifts (CLSs) of the Pt  $4f$ , O  $1s$ , and N  $1s$  states were obtained as a function of the NO coverage. In comparison to Pt  $4f$  state of the clean Pt(111) surface, a positive CLS of 0.2 eV was found at low NO exposures. With increase of the NO exposures, a second

peak at higher binding energy of 0.5 eV appears. Meanwhile, two O 1s peaks with difference of 1.7 eV were found and in contrast only one N 1s peak was found. When the Pt(111) surface was saturated by NO molecules, two Pt 4f peaks with CLS of 0.5 and 0.7 eV were found and the peak of 0.2 eV found at low coverage disappears. Correspondingly, the difference between two O 1s peaks decreases to 1.4 eV, but no discernible shift for N1s was found again.

The measured CLSs were interpreted by Zhu *et al.*<sup>9</sup> based on the available structure models mentioned above. The CLS results obtained for Pt 4f states and its dependence on the NO coverage can be well explained, however, the single N 1s level, which is constant regardless of the NO coverages, cannot be explained by those available models. For example, in the fcc+top configuration the N atoms have different coordination environments, i.e., threefold (fcc) and onefold (top) coordinated with the Pt atoms. Thus, the zero CLS of N 1s states is surprising as it is well known that CLS is very sensitive to the structure.<sup>18–25</sup> Therefore, these discrepancies indicate that further analysis of the NO/Pt(111) system is required, in particular, explicit CLS calculations by first-principles calculations are required, which has not been reported so far.

In this work, we performed an extensive density functional theory (DFT) investigation of the structure, energetics, and CLS of the NO/Pt(111) system at coverages of 0.25, 0.50, and 0.75 ML. Our results are in excellent agreement with available experimental results and a simple picture is suggested for the interaction of NO with Pt(111) surface. The CLS results of the Pt 4f states are well described by our calculations at different NO coverages, however, we found a large CLS of the N 1s states between top and hollow sites ( $\sim 0.7$  eV), irrespective of the coverage, which is in contrast to the zero (0 eV) shift found in XPS experiments. Our analysis indicates that the differences between our DFT calculations and the XPS measurements for the particular case of N and O 1s states may come from temperature effects. The rest of the paper is organized as follows. In Sec. II, we summarize the computational details. The structure and energetics are summarized in Sec. III while CLS results are analyzed in Sec. IV. In Sec. V, our main conclusions are summarized. Benchmark calculations are summarized in the Appendix.

## II. THEORETICAL APPROACHES AND COMPUTATIONAL DETAILS

Spin-polarized calculations were performed using DFT (Refs. 26 and 27) within the generalized gradient approximation (GGA)-Perdew-Burke-Ernzerhof (PBE) without statement otherwise.<sup>28</sup> The Kohn-Sham equations were solved using the ultrasoft-pseudopotential (USPP) plane-wave method,<sup>29</sup> as implemented in the DACAPO package.<sup>30</sup> For the CLS calculations, the relaxation of the core electrons, which may be important for open shell molecules NO, is not considered explicitly in USPP-DACAPO package. To include the relaxation of core electrons explicitly, we performed all-electron projected augmented-wave (PAW) calculations,<sup>31,32</sup> as implemented in the Vienna *Ab initio* Simulation Package

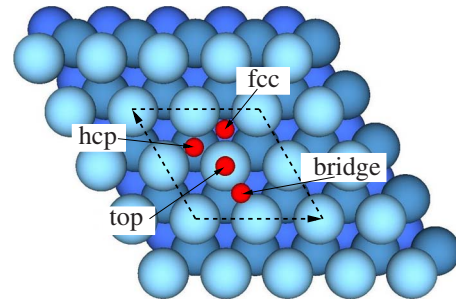


FIG. 1. (Color online) Top view of the high-symmetry adsorption sites (fcc, hcp, bridge, and top) on the Pt(111) surface. The  $(2 \times 2)$  unit cell is indicated by dashed lines. The Pt atoms and high-symmetry adsorption sites are indicated by large light blue balls and small red balls, respectively.

(VASP).<sup>33,34</sup> Our USPPs were generated using Vanderbilt's USPP generator with core cutoff radii  $r_c^N=0.6$  Bohr,  $r_c^O=0.7$  Bohr, and  $r_c^{Pt}=1.2$  Bohr. The valence electrons are described by 2s and 2p states for N and O with cutoff radii of  $r_s^N=r_p^N=r_s^O=r_p^O=1.3$  Bohr and 5d and 6s states for Pt with cutoff radii  $r_s=2.26$  Bohr,  $r_p=2.40$  Bohr, and  $r_d=2.00$  Bohr. The PAW projectors provided within VASP were used, which contains the same valence configuration as used for the USPPs. For the plane-wave expansion, cutoff energies of 350 eV (USPP) and 400 eV (PAW) were used, while for the Brillouin-zone integration, we employed for both methods the  $(12 \times 12 \times 1)$  and  $(6 \times 6 \times 1)$  Monkhorst-Pack **k**-point grids for the  $(1 \times 1)$  and  $(2 \times 2)$  unit cells,<sup>35</sup> respectively.

The Pt(111) surfaces were modeled using the repeated slab geometry, in which a seven-layer slabs are separated by a vacuum region of 16 Å. NO molecules were adsorbed on both sides of the slab. For all surface calculations, we used the theoretical equilibrium lattice constant of bulk Pt in the face-centered cubic structure,  $a_0$ . We found  $a_0=4.00$  Å (USPP) and 3.98 Å (PAW), while the experimental value is 3.92 Å,<sup>36</sup> i.e., overestimated by 2.0% (USPP) and 1.5% (PAW), as found commonly in DFT-GGA calculations.<sup>30,37–39</sup> As we will show below, NO adsorbed in the top sites are tilted away from the normal direction. To understand the role of the tilted angle in the adsorption properties, we employed the nudged elastic band (NEB) method to obtain the minimum-energy path from the tilted to the perpendicular configuration.<sup>40–42</sup> For all calculations, the NO molecules and the topmost two Pt layer were relaxed by minimizing the atomic forces up to  $0.02$  eV Å<sup>-1</sup>. All results reported below are obtained with the USPP-DACAPO without statements otherwise.

## III. RESULTS AND DISCUSSION

Experimental studies<sup>3,4,6–9</sup> have observed the formation of the  $(2 \times 2)$ -NO(fcc),  $(2 \times 2)$ -2NO(fcc+top), and  $(2 \times 2)$ -3NO(fcc+top+hcp) structures for NO/Pt(111) at  $\Theta_{NO}=0.25, 0.50$ , and 0.75 ML, respectively (see Fig. 2). Therefore, in this work, we considered only NO adsorption in  $(2 \times 2)$  structures. Our calculations show that the N-end down

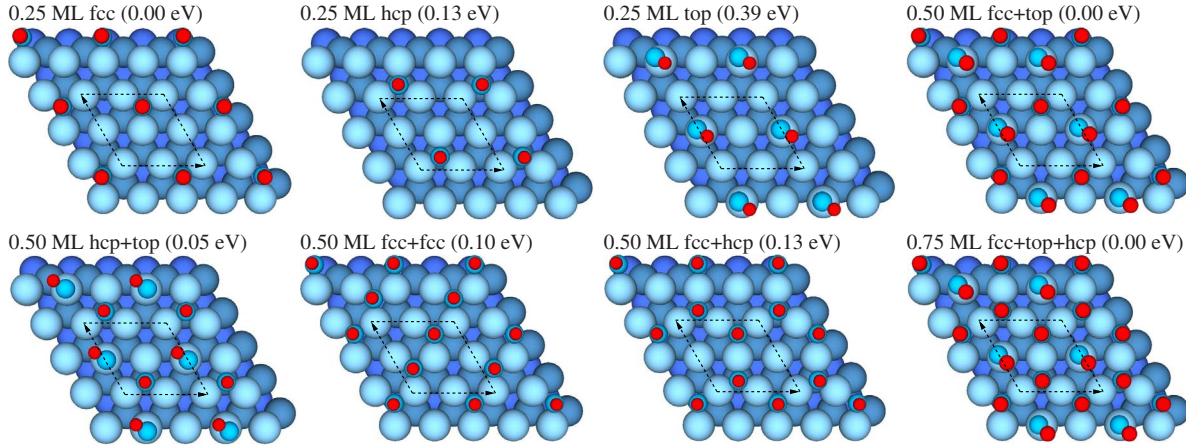


FIG. 2. (Color online) NO adsorption structures on Pt(111) in the  $(2 \times 2)$  unit cell (indicated by dashed lines) for different coverages and configurations. The Pt, N, and O atoms are indicated by large (light blue) balls, small blue, and red balls, respectively. The relative energy differences between different structures at given coverage are indicated in bracket.

configuration [N binds to the Pt(111)] is about 2.0 eV lower in energy than O-end configuration, which is consistent with experimental results.<sup>3,4,8</sup> In the following, only N-end down configurations were considered. Calculations were performed for  $\Theta_{\text{NO}}=0.25, 0.50$  and  $0.75$  ML, in which the NO molecules are adsorbed at the high-symmetry sites, namely, fcc, hcp, top, and bridge for 0.25 ML (see Fig. 2), as well as on the combinations among the adsorption sites (fcc+hcp, fcc+top, fcc+top+hcp, etc.) at higher coverages.

### A. Clean Pt(111) surface and NO in gas phase

#### 1. Clean Pt(111) surface

We found a slight expansion of the topmost interlayer spacing,  $\Delta d_{12}=+1.05\%$ , while the second interlayer spacing,  $\Delta d_{23}$ , contracts by  $-0.15\%$  compared to the truncated bulk Pt(111) interlayer spacing ( $d_0=2.31$  Å). These results are in good agreement with previous DFT-GGA calculations, e.g.,  $\Delta d_{12}=+1.14\%,^{39} +0.94\%,^{43}$   $\Delta d_{23}=-0.29\%,^{39}$  as well as with LEED studies, e.g.,  $\Delta d_{12}=+1.0 \pm 0.1\%,^{44}$   $+0.9 - +1.1\%.^8$  We found a work function,  $\Phi$ , of 5.75 eV, which deviates by less than 0.10 eV from previous DFT-GGA results, e.g., 5.69 eV (Ref. 39) and 5.80 eV,<sup>45</sup> and it is in good agreement with experimental results.<sup>46-48</sup>

#### 2. NO in gas phase

We obtained an equilibrium bond length of 1.18 Å, which is 2.6% larger than the experimental value of 1.15 Å (Ref. 49) and in good agreement with previous calculations (1.17 Å).<sup>12,16</sup> We obtained a NO stretch vibration of  $1946$   $\text{cm}^{-1}$ , which is only 2.2% larger than the experimental value of  $1904$   $\text{cm}^{-1}$ .<sup>49</sup> Furthermore, it is in good agreement with previous DFT-GGA calculations, e.g.,  $1917$   $\text{cm}^{-1}$  (Ref. 16) and  $1906$   $\text{cm}^{-1}$ .<sup>12</sup> The DFT-PBE electronic structure of NO is shown in Fig. 3(c), in which both highest occupied molecular orbital (HOMO) and lowest unoccupied molecular orbital (LUMO) are  $\pi^*$  states. Electronic states obtained by hybrid DFT within the PBE0 functional,<sup>50-53</sup> in which 25% of exact nonlocal exchange is added to the PBE functional,

are also shown [Fig. 3(b)]. As expected, PBE underestimates the HOMO-LUMO gap compared to the PBE0 result.

### B. Energetics

The adsorption energies are calculated as an average over different adsorption sites,  $E_{\text{ad}}^{\text{ave}}$ , or energy gain of the specific adsorption site with respect to the preadsorbed NO, so-called differential adsorption energy,<sup>54,55</sup>  $E_{\text{ad}}^{\text{diff}}$ . The average adsorption energy is given by

$$E_{\text{ad}}^{\text{ave}} = (E_{\text{tot}}^{\text{NO/Pt(111)}} - E_{\text{tot}}^{\text{Pt(111)}} - N_{\text{NO}}E_{\text{tot}}^{\text{NO}})/N_{\text{NO}}, \quad (1)$$

where  $E_{\text{tot}}^{\text{NO/Pt(111)}}$ ,  $E_{\text{tot}}^{\text{Pt(111)}}$ , and  $E_{\text{tot}}^{\text{NO}}$  are the total energies of NO/Pt(111), clean Pt(111) surface, and NO in gas phase, respectively.  $N_{\text{NO}}$  is the number of NO in the  $(2 \times 2)$  unit cell, in which NO molecules are adsorbed symmetrically on both sides of the slab. The differential adsorption energy of NO in the top at 0.50 ML,  $(2 \times 2)$ -2NO(fcc+top), is calculated as follows:

$$E_{\text{ad}}^{\text{diff}}(\text{top}) = (E_{\text{tot}}^{\text{fcc+top}} - E_{\text{tot}}^{\text{fcc}} - 2E_{\text{tot}}^{\text{NO}})/2. \quad (2)$$

For  $\Theta_{\text{NO}}=0.25$ , the average and differential adsorption energies have the same value. The calculated  $E_{\text{ad}}^{\text{ave}}$  and  $E_{\text{ad}}^{\text{diff}}$  for the configurations shown in Fig. 2 are summarized in Table I

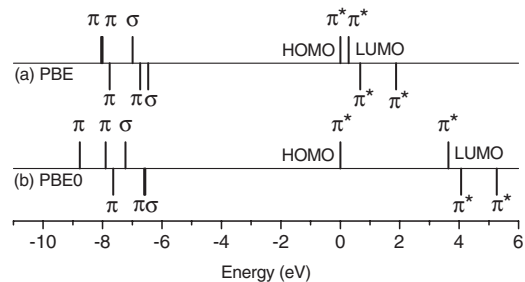


FIG. 3. (a) Electronic structure of NO in gas phase using DFT-PBE and (b) hybrid-DFT within the PBE0 functional. The highest occupied and lowest unoccupied molecular orbitals (HOMO, LUMO) are indicated along with the  $\pi$  and  $\sigma$  orbitals.

TABLE I. Differential,  $E_{\text{ad}}^{\text{diff}}$ , and average,  $E_{\text{ad}}^{\text{ave}}$ , adsorption energies for NO/Pt(111) in the  $(2 \times 2)$  structure.

$\Theta_{\text{NO}}$ (ML)	Structure	$E_{\text{ad}}^{\text{diff}}$ (eV)				$E_{\text{ad}}^{\text{ave}}$ (eV)
		fcc	hcp	Top (t)	Top (p)	
0.25		-1.84	-1.71	-1.45		
		-1.75 <sup>a</sup>	-1.66 <sup>a</sup>		-0.64	
		-2.09 <sup>b</sup>	-1.92 <sup>b</sup>	-1.61 <sup>b</sup>		
		-1.85 <sup>c</sup>	-1.76 <sup>c</sup>		-0.81	
		-2.10 <sup>d</sup>	-1.97 <sup>d</sup>	-1.69 <sup>d</sup>		
		-1.97 <sup>e</sup>	-1.83 <sup>e</sup>	-1.56 <sup>e</sup>		
0.50	fcc+top	-1.75		-1.36		-1.60, -1.82 <sup>b</sup>
	hcp+top		-1.65	-1.39		-1.55
	fcc+fcc	-1.16				-1.50, -1.71 <sup>b</sup>
	fcc+hcp	-1.23	-1.10			-1.47, -1.62 <sup>b</sup>
	0.75	fth <sup>g</sup>	-1.14	-1.03	-1.29	

<sup>a</sup>Reference 11, DFT-PW91 using pseudopotential method.

<sup>b</sup>Reference 12, DFT-PBE using USPP method implemented in STATE.

<sup>c</sup>Reference 14, DFT-PW91 using USPP method implemented in DACAPO.

<sup>d</sup>Reference 15, DFT-PW91 using USPP method implemented in DACAPO.

<sup>e</sup>Reference 16, DFT-PW91 using PAW method implemented in VASP.

<sup>f</sup>Reference 16, DFT-RPBE using PAW method implemented in VASP.

<sup>g</sup>fth=fcc+top+hcp

along with previous calculations for comparison.

For 0.25 ML, we found that NO preferentially binds to the fcc site ( $E_{\text{ad}} = -1.84$  eV), which is 0.13 and 0.39 eV lower in energy than the hcp and top sites, respectively. For 0.50 ML, the fcc+top configuration has the lowest energy ( $E_{\text{ad}}^{\text{ave}} = -1.60$  eV), which is 0.05, 0.10, and 0.13 eV lower in energy than the hcp+top, fcc+fcc, and fcc+hcp configurations, respectively. Similar energy differences were obtained using an unrelaxed Pt(111) slab, e.g., fcc+top is 0.11 eV lower in energy than the fcc+fcc structure. Thus, the relaxations of the topmost interlayer spacings cannot explain the stability of the fcc+top configuration, which is in contrast with Aizawa *et al.*<sup>12</sup> suggestion. The origin of the fcc+top preference will be discussed later. For fcc+top+hcp at 0.75 ML, we found  $E_{\text{ad}}^{\text{ave}} = -1.41$  eV. We noticed that the average adsorption energies decrease with the increase in the coverage, which indicates that there is a lateral repulsion between the adsorbates.

The adsorbate lowest energy structures, namely, fcc at 0.25 ML, fcc+top at 0.50 ML, and fcc+top+hcp at 0.75 ML are in excellent agreement with experimental results.<sup>3,4,6-10</sup> In this context, we note that the site preference for CO/Pt(111) at low coverage cannot be predicted correctly by DFT-GGA calculations (see Ref. 56 and references within). Thus, even that NO and CO differ only one electron, the performance of DFT-GGA to describe NO/Pt(111) is very different. To our best knowledge, explicit measurements of NO adsorption energies on Pt surfaces are only available for NO/Pt(110). Using microcalorimetric method, Wartnaby *et al.*<sup>57</sup> reported -1.66 eV for  $\Theta_{\text{NO}} < 0.25$  ML and -1.45 eV for  $\Theta_{\text{NO}} \approx 0.67$  ML, which are inline with our calculations (-1.84 and -1.41 eV at coverage of 0.25 and 0.75 ML).

The differential adsorption energies at 0.75 ML show the following trend,  $|E_{\text{ad}}^{\text{diff}}(\text{top})| > |E_{\text{ad}}^{\text{diff}}(\text{fcc})| > |E_{\text{ad}}^{\text{diff}}(\text{hcp})|$ . Namely, NO in the hcp sites is the least stable, and would desorb first with increase of the temperatures. This gives rise to the formation of the fcc+top configuration at 0.50 ML, in which there is a change in the order of the differential adsorption energies,  $|E_{\text{ad}}^{\text{diff}}(\text{top})| < |E_{\text{ad}}^{\text{diff}}(\text{fcc})|$ . Thus, further heating of NO/Pt(111) desorbs NO from the top sites and finally NO from the fcc sites (0.25 ML) desorb with clean Pt(111) left. Thus, the differential adsorption energies for hcp NO (1.03 eV, 0.75 ML), top NO (1.36 eV, 0.50 ML), and fcc NO (1.84 eV, 0.25 ML) agree well with distinct TPD peaks found in experiments.<sup>8,9</sup>

Our adsorption energy results are in good agreement with the results reported in Ref. 15, except that Ford *et al.*<sup>14</sup> found an adsorption energy of -0.81 eV for top NO at 0.25 ML due to the perpendicular configuration employed in their study. The present results are slightly different previous results,<sup>11,12,15,16</sup> which are mainly due to the differences in computational parameters. For example, three-layer slab was used in Ref. 15. Furthermore, the revised PBE (RPBE) functional yields smaller adsorption energies than the PW91 and PBE functionals, e.g., smaller by about 0.50 eV.<sup>30</sup> Nevertheless, all these calculations give exactly same site preference order. We note that the tilted top NO configuration was also obtained in previous NO/Pt(111) studies<sup>12,13,15,16</sup> and NO/Pd(111) at 0.25ML.<sup>58</sup>

### C. Geometric parameters

The geometric parameters defined in Fig. 4 are summarized in Table II along with the recent LEED results for

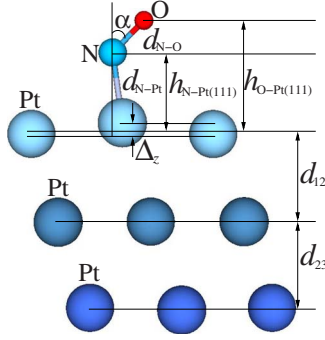


FIG. 4. (Color online) Side view of NO/Pt(111) for NO on the top site, in which the geometric parameters are indicated and listed in Table II.

comparison.<sup>8</sup> The Pt(111) surface is only slightly disturbed by NO, e.g.,  $\Delta d_{12}$  changes from +1.05% (clean surface) to +1.14 to +2.63%, while the buckling parameter,  $\Delta_z$ , is 0.16 Å for all the lowest energy structures. These results are in good agreement with LEED studies, which reported  $\Delta d_{12} = +1.77\%$  (0.25 ML),<sup>3,4,8</sup> and  $\Delta_z = 0.16$  Å (Ref. 8) and 0.07 Å,<sup>3,4</sup> respectively.

We found an increase in the bond length of NO,  $d_{N-O}$ , upon adsorption compared to NO in gas phase (1.18 Å),

e.g., at 0.25 ML,  $d_{N-O} = 1.21$  Å (hollow), and 1.19 Å (top). This result indicates a weakening of the N-O bond upon NO adsorption. The larger increasing for the hollow NO indicates a stronger interaction between the hollow NO and the substrate, which is consistent with the magnitude of the adsorption energies (Table I). The N-Pt bond lengths for NO in the hollow sites 2.10 Å are significantly larger than that in the top sites (1.96 Å) due to their different coordination numbers. As can be seen in Table II, our results are in excellent agreement with the LEED measurements at 90 K.<sup>8</sup>

For all structures, NO in the hollow sites are nearly perpendicular to the surface, i.e., tilted ( $\alpha$ ) angle smaller than  $0.1^\circ - 2.5^\circ$ , which is in good agreement with LEED results.<sup>3,4,8</sup> In contrast, NOs in the top sites are tilted significantly from the normal direction, e.g.,  $52.5^\circ$  (0.25 ML),  $50.2^\circ$  (0.50 ML), and  $45.7^\circ$  (0.75 ML). We noticed that  $\alpha$  decreases with increase of the coverage, however, LEED reported a slight increase in the tilted angle of NO in the top sites, e.g.,  $49.3^\circ$  (0.50 ML) and  $50.5^\circ$  (0.75 ML).<sup>8</sup>

It is important to point out that near-edge x-ray absorption fine spectroscopy studies suggested that NO in the hollow sites are tilted by  $20 \pm 5^\circ$  at 290 K and 0.25 ML,<sup>10</sup> which is in contrast with DFT calculations at zero temperature and LEED studies at 90 K.<sup>3,4,8</sup> At 0.50 ML, NEXAFS reported an upright NO in the hollow sites, while NO in the top sites are

TABLE II. Structural parameters for NO/Pt(111) with  $(2 \times 2)$  periodicity. Bond length of NO,  $d_{N-O}$ ; bond length between N and Pt,  $d_{N-Pt}$ ; perpendicular distance of N and O to the Pt(111) surface,  $h_{N-Pt(111)}$  and  $h_{O-Pt(111)}$ ; angle between the normal direction and the NO molecule,  $\alpha_{\perp-N-O}$ ; interlayer spacing relaxations,  $\Delta d_{ij}$ ; and buckling parameter,  $\Delta_z$ , as defined in Fig. 4. The experimental results (Ref. 8) are given in parentheses for comparison if available. The favorable adsorption configurations are indicated in bold font.

$\Theta_{NO}$ (ML)	Structures	Sites	$d_{N-O}$ (Å)	$d_{N-Pt}$ (Å)	$h_{N-Pt(111)}$ (Å)	$h_{O-Pt(111)}$ (Å)	$\alpha_{\perp-N-O}$ (degrees)	$\Delta d_{12}$ (%)	$\Delta d_{23}$ (%)	$\Delta_z$ (Å)
0.25	<b>fcc</b>	fcc	1.21 (1.19)	2.10 (2.07)	1.29 (1.31)	2.50 (2.50)	0.10 (0.00)	+2.63 (+1.77)	+0.71 (-0.44)	0.16 (0.08)
		hcp	1.21	2.11	1.37	2.58	0.00	+1.23	+0.48	0.14
		top	1.19	1.96	2.15	2.91	52.5	+2.29	-0.13	0.26
0.50	<b>fcc+top</b>	fcc	1.22 (1.21)	2.10 (2.01)	1.28 (1.22)	2.50 (2.43)	0.30 (2.0)	+1.14 (+2.93)	+1.15 (-0.18)	0.16 (0.08)
		top	1.18 (1.14)	1.98 (1.94)	2.13 (1.99)	2.89 (2.73)	50.2 (49.3)			
	hcp+top	hcp	1.22	2.11	1.32	2.53	0.80	+3.18	+0.37	0.25
		top	1.18	1.95	1.95	2.71	50.0			
	fcc+fcc	fcc	1.21	2.12	1.30	2.51	2.50	+3.52	+2.40	0.14
		fcc	1.21	2.12	1.30	2.51	2.50			
fcc+hcp	fcc	1.21	2.11	1.32	2.53	0.10	+4.30	+1.27	0.22	
	hcp	1.21	2.12	1.37	2.58	0.00				
0.75	<b>fcc+top+hcp</b>	fcc	1.22 (1.17)	2.11 (2.09)	1.32 (1.28)	2.53 (2.45)	0.50 (0.40)	+1.97 (+2.85)	+1.00 (+0.65)	0.16 (0.10)
		top	1.18 (1.12)	1.97 (1.99)	2.11 (2.05)	2.94 (2.76)	45.7 (50.5)			
		hcp	1.21 (1.15)	2.13 (2.01)	1.38 (1.34)	2.59 (2.53)	1.80 (0.10)			

TABLE III. Vibrational frequencies, in  $\text{cm}^{-1}$ , of NO on Pt(111) in the  $(2 \times 2)$  structure. The numbers in parentheses indicate the relative shift in percentage (%) compared to NO in gas phase theoretically ( $1946 \text{ cm}^{-1}$ ) and experimentally ( $1904 \text{ cm}^{-1}$ ) (Refs. 7 and 49).

$\Theta_{\text{NO}}$ (ML)		Adsorption sites					
		fcc		top		hcp	
0.25	USPP	1604	(-17.6%)	1781		1620	
	Exp.	1484	(-22.1%)				
0.50	USPP	1557	(-20.0%)	1792	(-7.9%)		
	Exp.	1430	(-24.4%)	1715	(-9.9%)		
0.75	USPP	1582	(-18.7%)	1785	(-8.3%)	1609	(-17.3%)
	Exp.	1444	(-23.6%)	1710	(-10.1%)	1508	(-20.8%)

tilted by  $50 \pm 10^\circ$  (Ref. 10) and  $52 \pm 3^\circ$ .<sup>8</sup> Thus, those discrepancies between NEXAFS and LEED/DFT calculations indicate a dependence of the NO vibration and rotation on the temperatures.

#### D. Vibrational frequencies

The vibrational frequencies summarized in Table III were calculated employing the procedure outlined in Ref. 14. For NO in the fcc site, we found a N-O stretch frequency of  $1604 \text{ cm}^{-1}$  at 0.25 ML, which is  $342 \text{ cm}^{-1}$  (-17.6%) smaller than the frequency of NO in gas phase ( $1946 \text{ cm}^{-1}$ ). By increasing the coverage, the frequency decreases to  $1557 \text{ cm}^{-1}$  (0.50 ML) and  $1582 \text{ cm}^{-1}$  (0.75 ML), which shows a modest dependence on coverage. We observed large changes with respect to the adsorption site, e.g.,  $1781 \text{ cm}^{-1}$  (top, 0.25 ML) compared to  $1604 \text{ cm}^{-1}$  (fcc, 0.25 ML), because of different coordination environment and binding mechanism. The significant redshift (in particular for NO in the hollow sites) upon adsorption shows a pronounced weakening of the N-O bond, which is consistent with the variation of the N-O bond lengths and adsorption energies. Our density of states and electron-density difference analyses (see Figs. 5 and 6) indicate that the weakening of the N-O bond is due to the charge back donation from the substrate to the NO  $2\pi^*$  antibonding orbital. Furthermore, it is important to men-

tion that the dipole-dipole interactions and substrate-mediated charge transfer might play a role.

Our calculated frequencies as well as their dependence on the coverage are in good agreement with experimental findings.<sup>7,59-62</sup> For example, experimental studies reported a redshift of wave number of about 22.1%, 24.4%, and 23.6% for NO in the fcc site at 0.25, 0.50, and 0.75 ML compared to NO in gas phase ( $1904 \text{ cm}^{-1}$ ), while the calculated values are 17.6%, 20.0%, and 18.7%, respectively. Previous first-principles calculations reported frequencies of  $1512 \text{ cm}^{-1}$  (Ref. 12) and  $1594 \text{ cm}^{-1}$ ,<sup>14</sup> for NO in the fcc site at 0.25 ML, which deviate from our calculations by 6.1% and 0.6%, respectively.

#### E. Work function

The change of the work function induced by the adsorption of NO on Pt(111) is discussed here. The magnitude and sign of  $\Delta\Phi$  can be used to obtain the direction and extent of the electron redistribution. The  $\Delta\Phi$  results are summarized in Table IV. The electronegativities of O and N atoms are significantly larger than that of the Pt atoms, e.g., Pauling electronegativities are 3.44, 3.04, and 2.28 for O, N, and Pt atoms respectively, and hence, a positive  $\Delta\Phi$  is expected on NO adsorption.<sup>63</sup> This is indeed found for NO in the hollow sites at 0.25 ML, e.g.,  $\Delta\Phi = 0.36 \text{ eV}$  (fcc) and  $0.24 \text{ eV}$  (hcp).

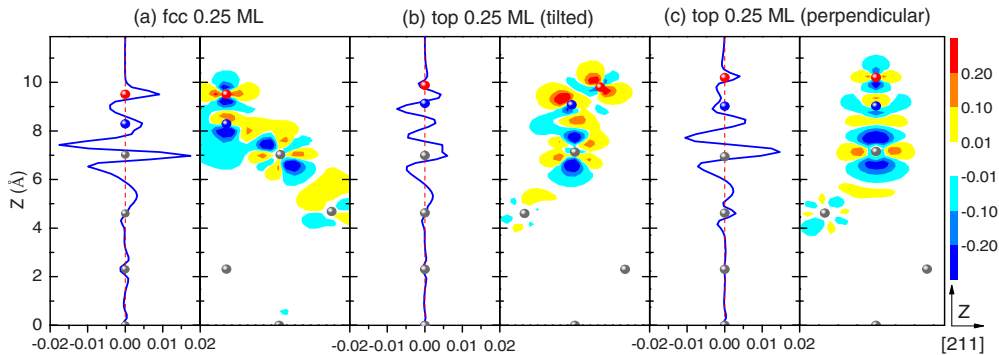


FIG. 5. (Color online) Planar average electron-density differences  $\bar{\rho}^\Delta(\mathbf{z})$  and electron-density differences  $\rho^\Delta(\mathbf{r})$  along (211) planes for NO adsorbed on the (a) fcc, (b) top (tilted), and (c) top (perpendicular) sites at 0.25 ML. Cyan to blue (yellow to red) indicates the depletion (accumulation) of electron density. N, O, and Pt atoms are indicated by blue, red, and dark gray spheres, respectively. The unit is  $\text{\AA}^{-1}$  for  $\bar{\rho}^\Delta(\mathbf{z})$  and  $\text{\AA}^{-3}$  for  $\rho^\Delta(\mathbf{r})$ .

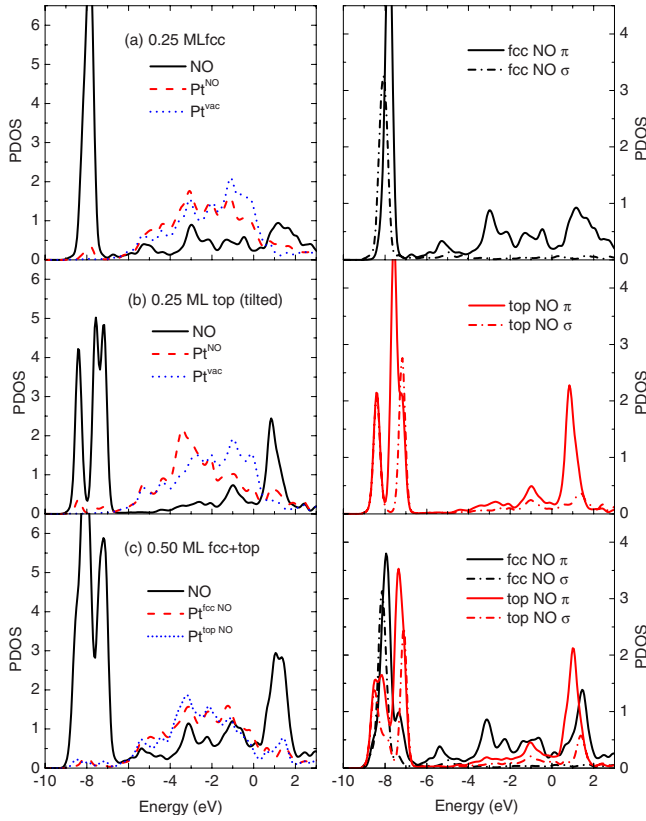


FIG. 6. (Color online) Projected density of states for NO/Pt(111) for (a) fcc and (b) top NO at 0.25 ML and (c) fcc+top (0.50 ML). In the left side, the total PDOS from adsorbed NO, bare surface Pt atoms ( $\text{Pt}^{\text{vac}}$ ), and surface Pt atoms coordinated with adsorbed NO (for instance  $\text{Pt}^{\text{NO}}$ ) are indicated. In the right side, the projected NO  $\sigma$  and  $\pi$  orbitals, defined in the main context, are plotted, respectively. The zero energy is the Fermi level.

However, it does not hold for NO in the top sites at 0.25 ML, for which we obtained  $\Delta\Phi = -0.35$  eV, i.e., a reduction of the work function. For perpendicular top NO,  $\Delta\Phi = -1.00$  eV. The opposite sign of  $\Delta\Phi$  for NO in the hollow and top sites at 0.25 ML comes from their different charge redistribution induced by adsorption, as discussed below.

The above results rationalize the variation of work function for NO adsorption at high coverages. For example, at 0.50 ML,  $\Delta\Phi = 0.03$  eV (fcc+top), which was found typically for physisorption systems such as Xe adsorption on graphite ( $\Delta\Phi = 0.10$  eV),<sup>64</sup> but not for chemisorption systems such as NO/Pt(111) with a significant binding energy of  $-1.60$  eV/NO for the fcc+top configuration. The small

TABLE IV. Work-function change,  $\Delta\Phi$  in eV, induced by NO adsorption on the Pt(111) in the  $(2 \times 2)$  structure.

0.25 ML	$\Delta\Phi$	0.50 ML	$\Delta\Phi$	0.75 ML	$\Delta\Phi$
fcc	0.36	fcc+top	0.03	fcc+top+hcp	0.19
hcp	0.24	hcp+top	-0.05		
top	-0.35	fcc+fcc	0.45		
		fcc+hcp	0.37		

value of  $\Delta\Phi^{\text{fcc+top}}$  is a result of the superposition over the adsorption of NO in the fcc and top sites, e.g.,  $\Delta\Phi^{\text{fcc}} + \Delta\Phi^{\text{top}} = 0.01$  eV. The same applies for the fcc+top+hcp configuration, i.e.,  $\Delta\Phi^{\text{fcc+top+hcp}} = 0.19$  eV, while we obtained 0.25 eV from the sum of the work functions for NO in the fcc, top, and hcp sites at 0.25 ML.

## F. Electron-density differences

To obtain insights into the mechanisms that yield a site-dependent work-function change, we analyzed the electron redistribution on NO/Pt(111). The electron-density differences,  $[\rho^\Delta(\mathbf{r}) = \rho^{\text{NO/Pt(111)}}(\mathbf{r}) - \rho^{\text{Pt(111)}}(\mathbf{r}) - \rho^{\text{NO}}(\mathbf{r})]$ , were calculated along with the plane (211) through the N and O atoms but perpendicular to the slab. Furthermore, we calculated also planar average electron-density differences,  $\bar{\rho}^\Delta(\mathbf{z})$ , along the normal direction ( $z$  axis). The plots are shown in Fig. 5 for the NO in the fcc, top (tilted), and top (perpendicular) sites at 0.25 ML.

The electron-density redistributions are located mainly in the topmost surface layer and adsorbed NO. For NO in the fcc sites [Fig. 5(a)], we observed a strong depletion and accumulation for the O  $p_z$  and  $(p_x, p_y)$  states, respectively. The charge redistribution on the N atoms shows a significant depletion of the N  $p_z$  states. For surface Pt atom bonded with adsorbed NO, corresponding  $d_{xz}$  states are depleted, while  $d_{z^2}$ ,  $d_{xy}$ , and  $d_{xx-yy}$  states increase. Compared to fcc NO, the charge redistribution for top NO is significantly different. For the perpendicular NO, there is considerable depopulation of the Pt  $d_{z^2}$  states, but becomes modest for the tilted NO. For both perpendicular and tilted configurations, we found an electron accumulation between NO and bonded Pt atom. Concerning N and O atoms in NO, we found that a charge increases around N for top NO, but increases mainly around O for fcc NO.

These trends can be seen from the averaged electron-density differences shown in Fig. 5. For example, there is strong depletion between the topmost Pt(111) layer and the N layer and large accumulation at the O position for NO in the fcc sites. However, there is no pronounced depletion between the Pt(111) and N layers for NO in the top sites found. Furthermore, there is a large charge increase around the N atoms. Thus, overall, the electron-density accumulation for NO in the top sites occurs near the Pt surface. To confirm this, we calculated the adsorption-induced dipole moment,  $\mu$ , using the procedure outlined in Ref. 65,

$$\mu = \int_0^{c/2} \bar{\rho}^\Delta(\mathbf{z}) z dz, \quad (3)$$

where  $\bar{\rho}^\Delta(\mathbf{z})$  is the planar averaged electron-density difference shown in Fig. 5. The integration is performed from the center of the slab to the center of the vacuum region. We found  $\mu = 0.60$  (0.26),  $-0.20$  ( $-0.25$ ), and  $-0.90$  Debye ( $-0.75$  Debye) for NO in fcc, top (tilted), and top (perpendicular), respectively. The induced dipole moments in parentheses were calculated for comparison using the Helmholtz equation,<sup>66,67</sup>  $\mu = 1/12\pi\Delta\Phi/\Theta_{\text{NO}}A$ , where  $A$  is the area per  $(1 \times 1)$  surface unit cell in  $\text{\AA}^2$ . Both approaches show clearly that  $\mu$  points downward to the surface for the fcc NO, but

upward to the vacuum for the top NO. Furthermore, the magnitudes of the induced dipole moments obtained by both approaches are in good agreement, except for NO in the fcc sites.

### G. Density of states

Further insights in the interaction between NO and Pt(111) can be identified using the projected density of states (PDOS). To visualize the hybridization between Pt bands and NO molecular orbitals, we define NO  $\sigma$ - and  $\pi$ - orbitals by summation of corresponding N and O  $p_{x,y}$  and  $p_z$ 's PDOS, namely,  $\pi=N_{p_x}+N_{p_y}+O_{p_x}+O_{p_y}$  and  $\sigma=N_s+N_{p_z}+O_s+O_{p_z}$ . The resulted NO's  $\pi$  and  $\sigma$  orbitals and surface Pt PDOS at different adsorption sites and coverages are shown in Fig. 6. For 0.25 ML NO adsorption at the hollow and top sites, the deep-lying NO  $\pi$  and  $\sigma$  are located at around  $-8$  eV with respect to the Fermi level and show only modest hybridization with Pt substrate. There are extensive hybridizations between NO  $\pi^*$  at the hollow sites and Pt in the energy range of  $[-6$  to  $3$  eV], which are inline with strong bonding between NO and Pt. While for the titled top NO, the contribution from NO  $\sigma$  increases, which is expected as in the top configuration the hybridization between NO  $\sigma$  and Pt  $5d_{z^2}$  is maximized. Meanwhile, the titled configuration for the top NO would facilitate the orbital hybridization between NO  $\pi^*$  and Pt  $5d_{xz,yz}$ , as seen clearly in Fig. 6(b). With increase of the coverage (fcc+top, 0.50 ML), the hybridization between adsorbed NO molecules and Pt substrates is enhanced and broadened due to the lateral interaction between the adsorbates mediated by the substrates.

To quantify the charge transfer induced by NO adsorption, we integrated corresponding NO's  $\sigma$  and  $\pi$  PDOS up to the Fermi level. In gas phase, NO has 11 electrons in the occupied valence states, in which six occupy  $\sigma$  states and five occupy  $\pi$  states, i.e., the highest occupied  $\pi$  state is only half occupied. These occupations were used as reference. For 0.25 ML, the occupations of the NO  $\pi$  orbitals are 5.47 (fcc), 5.39 (top), and 5.45 $e$  (hcp). For fcc+top configuration at 0.50 ML, the results are 5.50 (fcc) and 5.38 $e$  (top), and 5.50 (fcc), 5.37 (top), and 5.45 $e$  (hcp) for fcc+top+hcp configuration at 0.75 ML, respectively. Thus, our analysis indicates clearly a pronounced charge transfer from the substrate to NO  $\pi$  states upon NO adsorption. In contrast, the population of the NO  $\sigma$  states decreases upon adsorption. For example, we obtained 5.78 (fcc), 5.82 (top), and 5.79 $e$  (hcp) at 0.25 ML, 5.78 (fcc) and 5.82 $e$  (top) at 0.50 ML (fcc+top), and 5.78 (fcc), 5.84 (top), and 5.81 $e$  (hcp) at 0.75 ML (fcc+top+hcp). Thus, a charge transfer from the NO  $\sigma$  states to substrate can be recognized.

This analysis shows that the interaction between NO and Pt(111) follows the donation-back-donation model, as well established for CO/Pt(111).<sup>56,68-76</sup> Our results show a modest site dependence of the magnitudes of the donated and back-donated electrons, e.g., the  $\sigma$  states donate 0.18 $e$  (0.25 ML, top) and 0.22 $e$  (0.25 ML, hollow) to the substrate. The back donation from the substrate to the NO  $\pi$  states is 0.39 $e$  (0.47 $e$ ) for the top (hollow) sites. The larger donation and back donation for NO in the hollow sites than that in the top

sites are inline with its stronger bond strength with the substrate. The preference of the hollow sites also rationalizes the tilted configuration for the top NO, which would facilitate the donation and back-donation processes, as seen clearly from Fig. 6(b).

Independent of the NO coverage and adsorption sites, we found that the charge donation from NO to substrate is smaller than the back-donation process. Thus, it leads to a net charge transfer from the substrate to the adsorbate, namely, 0.25 (fcc), 0.21 (top), and 0.23 $e$  (hcp) at 0.25 ML; 0.28 (fcc) and 0.20 $e$  (top) at 0.50 ML (fcc+top); 0.28 (fcc), 0.21 (top), and 0.26 $e$  (hcp) at 0.75 ML (fcc+top+hcp). Despite the overall charge transfer, the detailed charge redistributions are site dependent, as discussed in above, which determines the sign of the surface work-function change and dipole moment, correspondingly.

The mechanism proposed above also rationalizes the structures formed at higher coverage, for example, fcc+top and/or hcp+top configurations (0.50 ML), instead of fcc+fcc and fcc+hcp configurations. For the latter two configurations, there is one Pt atom shared by two adsorbed NOs, which limits the amount of charge transfer from the substrate to the adsorbed NO due to the site competition. On the other hand, the opposite sign of the dipole moment between top and hollow sites minimizes the electrostatic repulsion between adsorbed NO molecules, which is not the case for the fcc+fcc and/or fcc+hcp configurations.

### IV. CORE-LEVEL SHIFTS

The relative shift in the core-level binding energies is element specific and sensitive to the local geometries. Thus, XPS measurements of CLSs have been widely used as a fingerprint to help in the identification of the adsorbates, adsorption sites, and valence states.<sup>18,22-25,77-79</sup> CLSs are calculated as the energy difference between the specific core-level binding energy of the excited atom ( $E_{cl}^i$ ) and the reference atom ( $E_{cl}^{ref}$ ), i.e.,  $CLS=E_{cl}^i-E_{cl}^{ref}$ . In this work, the final-state approximation<sup>23,77</sup> was used to calculate core-level binding energy by the total-energy difference between two configurations, namely, an excited configuration in which an electron is removed from a specific core state,  $E_{tot}(n_c-1)$ , and the ground-state configuration,  $E_{tot}(n_c)$ . Thus,  $E_{cl}=E_{tot}(n_c-1)-E_{tot}(n_c)$ , in which the core hole is assumed to remain localized in the excited atom.

The USPP and the all-electron PAW methods were used to calculate the CLSs. In the USPP method, the excited atom is described by a new USPP, which is generated by removing the target core electron from the isolated atom.<sup>18,22,23,78,79</sup> In the PAW method, a core electron is removed from the core by generating the corresponding core excited ionic PAW potential in the course of the calculation and remaining core states are relaxed along of the self-consistent calculation.<sup>23-25,33</sup> The all-electron PAW method is expected to provide higher accuracy due to the explicit relaxation of the core electrons.<sup>33</sup>

#### A. CLS: Pt 4f state

The CLSs of the Pt 4f states in the topmost surface layer due to the adsorption of NO are summarized in Fig. 7 along

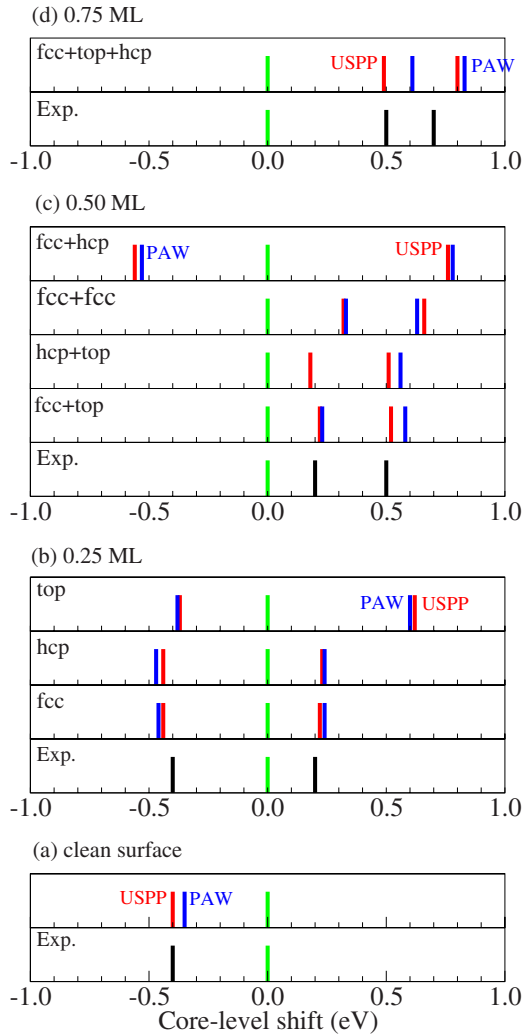


FIG. 7. (Color online) CLSs of the Pt 4f states in the topmost Pt(111) layer. (a) Clean surface. NO adsorption on Pt(111) for (b)  $\Theta_{\text{NO}}=0.25$ , (c) 0.50 ML, and (d) 0.75 ML. The CLSs are given with respect to the bulk Pt atoms (center layer in the slab) and indicated by green lines. The USPP and PAW results are indicated in red and blue, respectively, while the experimental results (Ref. 9) are in black.

with the experimental results.<sup>9</sup> The CLSs of surface Pt atoms are given with respect to the center Pt layer in the seven-layer slab. For NO/Pt(111), the Pt atoms can be divided in two groups, namely, Pt atoms coordinated with the N atoms ( $\text{Pt}^{\text{NO}}$ ) and Pt atoms not coordinated with any N atoms ( $\text{Pt}^{\text{vac}}$ ). For the clean Pt(111) surface, the CLSs for the topmost surface atoms are  $-0.40$  eV (USPP) and  $-0.38$  eV (PAW), which are in good agreement with the experimental values of  $-0.4$  eV (Ref. 9) and  $-0.42$  eV.<sup>78</sup>

For 0.25 ML, the averaged CLSs of the  $\text{Pt}^{\text{vac}}$  atoms for NO in the fcc and hcp sites are  $-0.44$  eV (USPP) and  $-0.47$  eV (PAW), which shows only a modest change with respect to the  $\text{Pt}^{\text{vac}}$  from the clean surface. For Pt atoms coordinated with the adsorbed hollow NO, we found a positive shift of 0.23 eV (USPP) and 0.24 eV (PAW). In contrast, there is a significant shift of 0.62 eV (USPP) and 0.60 eV (PAW) for  $\text{Pt}^{\text{NO}}$  coordinated with the top NO. Experimental

studies<sup>9</sup> reported two XPS peaks with shifts of  $-0.40$  and  $0.20$  eV. By comparing to our calculations, these two peaks should correspond to the  $\text{Pt}^{\text{vac}}$  and Pt atoms coordinated with NO in the hollow sites, respectively. Since NO in the fcc sites is energetically more favorable than the hcp sites (see Table I), hence, the peak at 0.20 eV was attributed to the Pt atoms coordinated to the fcc NO, accordingly.

At 0.50 ML, the calculated CLS results for both fcc+top and hcp+top configurations agree well with the experiment results.<sup>9</sup> Thus, fcc+hcp and fcc+fcc structures can be excluded safely as possible structures for NO/Pt(111) at 0.50 ML, which is consistent with their higher energetics (Table I). The adsorption energy for hcp+top is less favorable than fcc+top by 0.10 eV per  $(2 \times 2)$  cell and hence, the former one can be excluded. For the fcc+top structure, all surface Pt atoms are coordinated with NO molecules: three of the four Pt atoms are coordinated with one NO in the fcc sites and have a CLS of 0.20 eV, while the fourth Pt atom is coordinated with NO in the top sites and has a CLS of 0.50 eV. At 0.75 ML, one additional NO adsorbs to form the fcc+top+hcp configuration. The three Pt atoms that coordinated with two NO in the hollow sites have CLS of 0.49 eV (USPP) and 0.60 eV (PAW), while we found 0.80 eV (USPP) and 0.83 eV (PAW) for the fourth Pt atom coordinated with NO in the top sites. These results are consistent with experimental results (0.50 and 0.70 eV).<sup>9</sup>

The good agreement between our CLS calculations and the experiments for the Pt 4f states provides a strong support of the  $(2 \times 2)$ -NO(fcc),  $(2 \times 2)$ -2NO(fcc+top), and  $(2 \times 2)$ -3NO(fcc+top+hcp) structure models as proposed by total-energy calculations. The agreement justifies further the theoretical approach employed in this work. On the other hand, the strong dependence of the CLS of Pt 4f states on the coordination indicates a dominant contribution from the initial states to the CLS, as concluded similarly for other transition-metal surfaces.<sup>79</sup>

## B. CLS: N and O 1s-states

In this section, we discuss the CLS results for the N and O 1s states upon NO adsorption. The CLSs are given with respect to the NO in the fcc sites at the corresponding coverage. We found a zero shift of the N and O 1s states between fcc and hcp NOs in the fcc+top+hcp and fcc+hcp configurations, which is expected as both hollow sites have the same threefold coordination. This is consistent with the experiments,<sup>9</sup> where only two distinct O 1s peaks were reported for fcc+top+hcp. Below, only the CLS for NO in the top sites with respect to the hollow sites is discussed. For fcc+top, we obtained  $\text{CLS}_{\text{N}}=-0.78$  eV (USPP),  $-0.79$  eV (PAW) and  $\text{CLS}_{\text{O}}=1.04$  eV (USPP), 1.14 eV (PAW) for NO in the top sites. For fcc+top+hcp, we obtained  $\text{CLS}_{\text{N}}=-0.72$  eV (USPP),  $-0.71$  eV (PAW) and  $\text{CLS}_{\text{O}}=1.02$  eV (USPP), 1.12 eV (PAW), respectively. Both methods give similar results with differences of less than 0.10 eV, which indicates that the effect of core relaxation is modest for NO/Pt(111). These contrast to the experiments with single N 1s peaks regardless to the coverages and two distinct O 1s peaks with relative shift of 1.70 eV (0.50 ML) and 1.40 eV

(0.75 ML).<sup>9</sup> However, we note that compared to the experiments, both N and O 1s CLSs for the top NO with respect to the fcc NO are shifted consistently to lower binding by about 0.7 eV.

Since CLS are very sensitive to the geometry, we optimized the structures using higher computational parameters to exclude possible numerical errors. The cutoff energy was increased to 450 eV and a  $k$ -point grid of  $(8 \times 8 \times 1)$  for the  $(2 \times 2)$  structure was employed, however, the variation is less than  $\pm 0.01$  eV. To exclude possible artificial Coulomb repulsion between ionic atoms introduced by the limited  $(2 \times 2)$  cell, larger  $(4 \times 4)$  unit cells were used, in which only one NO every four top NO molecules is excited. The variation of the results is modest. We check further possible excitation-induced structural change and found that the effects on the structures and CLSs are small and can be excluded too. Finally, we also test the USPP and PAW potentials used for the nitrogen atom in different N-containing molecules in gas phase including NO, NO<sub>2</sub>, N<sub>2</sub>, NH<sub>3</sub>, and HCN in gas phase with respect to the N<sub>2</sub>. The results are given in the Appendix and a good agreement with available experimental results can be found.

The large differences between calculated and measured N and O 1s states may lie in the lack of a proper description of the interaction and geometry of NO and Pt(111) by present DFT-PBE and affect the CLS results, correspondingly. Indeed, the effect of the exchange-correlation functional on the adsorption has been widely discussed in literatures. For example, it is well documented that DFT-GGA yields the wrong adsorption site preference for the CO adsorption on Pt(111) at lower coverages. Due to the underestimation of the LUMO CO favors artificially the hollow sites.<sup>56,68–76</sup> Since DFT-PBE also underestimates the HOMO-LUMO energy separation for NO in gas phase (see Fig. 3), it may affect the NO adsorption on Pt(111) and corresponding geometries and CLS. Our calculations however rule out this possibility. In this context, we note first that the present DFT-PBE yields the correct NO adsorption site on Pt(111) at coverages of 0.25, 0.50, and 0.75 ML and the optimized geometric parameters are in good agreement with LEED and STM results.<sup>3,4,6–8</sup> Furthermore, we optimized the fcc+top configuration using four-layer slab by the hybrid-functional PBE0 as implemented in VASP 5.1. We found that the geometries are essentially same as the one obtained using the PBE functional. Specifically the tilted angle of top NO changes only by 3°. Therefore, the effect of the underestimation of the NO HOMO-LUMO gap by the PBE on CLS can be excluded. Compared to CO, the half-filled NO  $\pi^*$  orbital makes the charge transfer from the substrate to NO facile and therefore the consequence of the underestimation of the NO HOMO-LUMO gap is less prominent.

As mentioned in Sec. III C, there is considerable error bar in the measured titled angle of the top NO. For example, NEXAFS studies performed at 290 K found that the hollow NO tilted angle at 0.25 ML is as large as 20°. For  $\Theta = 0.50$  ML, experiments found that fcc NO is upright and top NO is tilted with error bar of about 10°.<sup>3,4,8,10</sup> On the other hand, DFT calculations have been performed at absolute zero and found fcc NO is always upright. To study the possible temperature effects, we performed molecular-dynamics

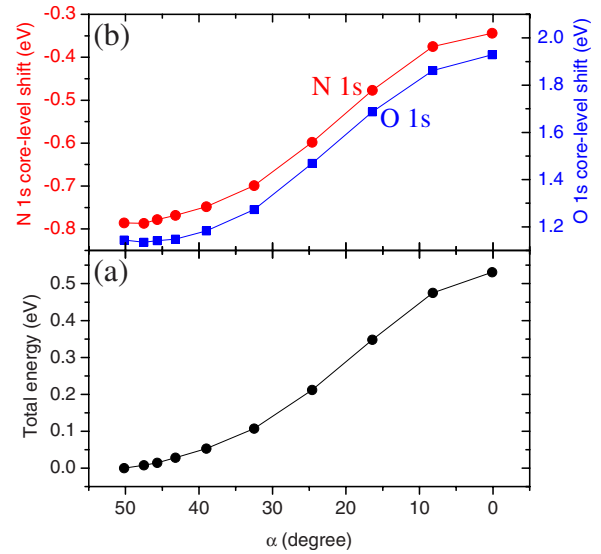


FIG. 8. (Color online) NO adsorption on Pt(111) in the  $(2 \times 2)$ -2NO(fcc+top) structure. (a) Total energy and (b) core-level shift of the N and O 1s states as a function of the tilted angle ( $\alpha = 0$ – $50.2^\circ$ ) for NO in the top sites (see Fig. 4).  $\alpha = 0$  corresponds to optimized perpendicular top NO and  $\alpha = 50.2^\circ$  for optimized tilted configuration.

(MD) simulation for the fcc+top configuration at  $T = 300$  K. The simulations indeed show that NO in the top sites changes the tilted angle by about  $10^\circ$  and more important fcc NOs become tilted with angle of about  $10^\circ$ . The details will be discussed elsewhere.

The effects of the tilted angle of the top NO on the energy and CLS were studied by exploring the potential-energy surface using NEB, where the optimized tilted ( $50.2^\circ$ ) and perpendicular top NOs of fcc+top configuration were used as the initial and final states. As plotted in Fig. 8, both of the total energy and the CLS show strong dependence on the tilted angle. When  $\alpha$  varies from  $50.2^\circ$  to  $16.4^\circ$ , the total energy increases gradually, while N 1s CLS changes from  $-0.79$  to  $-0.34$  eV, and O 1s changes from 1.14 to 1.69 eV. These results show that the top NO with smaller tilted angles yields N and O 1s CLSs closer to the experimental values. Furthermore, our calculation shows that for perpendicular top NO, a small decrease of the distance between N and Pt yields a zero N 1s CLS, while O 1s CLS changes by 0.1 eV. At finite temperatures, adsorbed NO molecules may vibrate and/or rotate along the normal direction, as indeed found from our MD simulations. The sensitivity of the CLS versus the titled angle and the distance between NO and Pt found indicate that the discrepancy between present DFT calculations and measurements at typically room temperatures may come from the thermal motion of adsorbed molecules. To clarify this issue, XPS measurements at low temperatures would be very helpful.

## V. SUMMARY

In this work, we reported a systematic DFT-PBE study of the NO adsorption on the Pt(111) surface at 0.25, 0.50, and

0.75 ML. The energetically most favorable adsorption configuration with periodicity of the  $(2 \times 2)$  structures fcc (0.25 ML), fcc+top (0.50 ML), and fcc+top+hcp (0.75 ML), as well as their geometries optimized are in excellent agreement with the experiments and previous DFT calculations. Significant redshift of the N-O stretch upon NO adsorption on Pt(111) was found and compared to top NO, the redshift for the hollow NO is larger.

It was found that the bonding between NO and Pt(111) follows the donation–back-donation mechanism, in which the NO  $\sigma$  states donate electrons to the substrate Pt  $d$  states, which back donate further to the NO  $\pi$  states. There is a net charge from the substrate to the adsorbate regardless to the adsorption sites and coverages. However, electron-density differences on NO adsorption indicate that the transferred electron accumulates mainly around the nitrogen atoms for NO in the top sites, but accumulates around the oxygen atoms for NO in the fcc sites. The site dependence of the charge rearrangement explains the opposite sign of the dipole moment induced by NO adsorption in the top and hollow sites.

For NO adsorption at coverage of 0.50 ML, we found that fcc+top configuration is favorable because the absence of the site competition, which occurs for fcc+fcc or fcc+hcp configurations otherwise. On the other hand, the opposite dipole moment between fcc NO and top NO minimizes the electrostatic repulsion between adsorbed NO molecules. At higher coverage, NO starts to populate the hcp hollow sites.

We found that the CLS of the Pt  $4f$  states is very sensitive to the local geometries and the number of coordinated NO molecules. The agreement between calculated and measured CLSs of Pt  $4f$  in the range of coverage considered is excellent. The agreement not only corroborates the structural models studied, but also justifies the methodology used, which may be generalized to more complex reaction conditions and other transition-metal surfaces. Meanwhile, there are significant difference between calculated and measured CLS for N and O  $1s$  levels. The effects of the exchange-correlation functional and core-hole relaxation can be excluded. Instead, our study indicates that the thermal vibration and rotation may be responsible and call for XPS measurements at low temperatures.

#### ACKNOWLEDGMENTS

We thank Wenhua Zhang and Yi Luo for fruitful discussions. We acknowledge the financial support from the Natural Science Foundation of China (Contracts No. 20503030, No. 20733008, and No. 20873142) and the National Basic Research Program of China (Contract No. 2007CB815205).

#### APPENDIX: BENCHMARK TESTS

To benchmark the methodology of the present CLS calculations, we calculated the CLS of the N  $1s$  level for a se-

TABLE V. Equilibrium bond lengths,  $d_{A-B}$  in Å, and angles,  $\alpha_{B-A-B}$  in degrees. The numbers in parentheses indicate the deviation in percentage (%) with respect to experimental results (Ref. 49).

		USPP	PAW	Expt.
NO	$d_{N-O}$	1.177 (2.53)	1.172 (2.09)	1.148
NO <sub>2</sub>	$d_{N-O}$	1.216 (1.93)	1.214 (1.76)	1.193
	$\alpha_{O-N-O}$	134.0 (−0.07)	133.2 (−0.67)	134.1
N <sub>2</sub>	$d_{N-N}$	1.120 (2.00)	1.117 (1.73)	1.098
NH <sub>3</sub>	$d_{N-H}$	1.025 (1.28)	1.024 (1.19)	1.012
	$\alpha_{H-N-H}$	106.8 (0.14)	106.4 (−0.29)	106.7
HCN	$d_{C-N}$	1.161 (0.43)	1.162 (0.52)	1.156
	$d_{C-H}$	1.074 (0.94)	1.076 (1.13)	1.064

lected set of molecules (N<sub>2</sub>, NO, NO<sub>2</sub>, HCN, and NH<sub>3</sub>), in which the CLS are given with respect to the N<sub>2</sub>. To do so, we employed a orthorhombic box with size of  $15 \times 15.5 \times 16$  Å<sup>3</sup> and a single  $\mathbf{k}$  point (0.25,0.25,0.25) for the Brillouin-zone integration. The optimized equilibrium parameters are summarized in Table V with the experimental results.<sup>49</sup> The largest deviation between theory and experiment results is 2.09%, which shows the good accuracy of our calculations. In Table VI, we summarize the CLS results and compare to the experiments.<sup>80</sup> The USPP and PAW results are in quite good agreement with the experiments, i.e., the largest deviations are 0.48 and 0.26 eV for NO<sub>2</sub>, respectively. From these calculations, we can see that (i) both methods yield essentially the same equilibrium bond lengths with differences of less than 0.01 Å and (ii) the CLS results obtained by the PAW method for the molecules in gas phase are in better agreement with the experiments.<sup>80</sup> As discussed in Sec. IV, the agreement between the USPP and PAW methods for the clean Pt(111) is excellent, which can be attributed to the efficient screening of the core hole in metals. This is however worse for molecular systems, in which the core-hole relaxation may be important and requires the more reliable methods. For adsorbate-substrate system, as studied in present NO/Pt, the error bar introduced may be improved and slightly better than isolated molecules.

TABLE VI. Core-level shift (N  $1s$  state) of molecular systems with respect to the N  $1s$  of N<sub>2</sub> (in eV).

	USPP	PAW	Expt. <sup>a</sup>
NO	0.90	0.90	0.8
NO <sub>2</sub>	2.52	2.74	3.0
N <sub>2</sub>	0.00	0.00	0.00
NH <sub>3</sub>	−4.48	−4.31	−4.3
HCN	−3.22	−3.13	−3.1

<sup>a</sup>Experimental results from Ref. 80.

\*Authors to whom correspondence should be addressed.

- <sup>1</sup>B. E. Nieuwenhuys, *Adv. Catal.* **44**, 259 (1999).
- <sup>2</sup>J. Kašpar, P. Fornasiero, and N. Hickey, *Catal. Today* **77**, 419 (2003).
- <sup>3</sup>N. Materer, A. Barbieri, D. Gardin, U. Starke, J. D. Batteas, M. A. VanHove, and G. A. Somorjai, *Phys. Rev. B* **48**, 2859 (1993).
- <sup>4</sup>N. Materer, A. Barbieri, D. Gardin, U. Starke, J. D. Batteas, M. A. Vanhove, and G. A. Somorjai, *Surf. Sci.* **303**, 319 (1994).
- <sup>5</sup>F. Esch, T. Greber, S. Kennou, A. Siokou, S. Ladas, and R. Imbihl, *Catal. Lett.* **38**, 165 (1996).
- <sup>6</sup>M. Matsumoto, N. Tatsumi, K. Fukutani, T. Okano, T. Yamada, K. Miyake, K. Hate, and H. Shigekawa, *J. Vac. Sci. Technol. A* **17**, 1577 (1999).
- <sup>7</sup>M. Matsumoto, K. Fukutani, T. Okano, K. Miyake, H. Shigekawa, H. Kato, H. Okuyama, and M. Kawai, *Surf. Sci.* **454-456**, 101 (2000).
- <sup>8</sup>M. Matsumoto, N. Tatsumi, K. Fukutani, and T. Okano, *Surf. Sci.* **513**, 485 (2002).
- <sup>9</sup>J. F. Zhu, M. Kinne, T. Fuhrmann, R. Denecke, and H. P. Steinrück, *Surf. Sci.* **529**, 384 (2003).
- <sup>10</sup>P. Zhu, T. Shimada, H. Kondoh, I. Nakai, M. Nagasaka, and T. Ohta, *Surf. Sci.* **565**, 232 (2004).
- <sup>11</sup>Q. Ge and D. A. King, *Chem. Phys. Lett.* **285**, 15 (1998).
- <sup>12</sup>H. Aizawa, Y. Morikawa, S. Tsuneyuki, K. Fukutani, and T. Ohno, *Surf. Sci.* **514**, 394 (2002).
- <sup>13</sup>R. Burch, S. T. Daniells, and P. Hu, *J. Chem. Phys.* **117**, 2902 (2002).
- <sup>14</sup>D. C. Ford, Y. Xu, and M. Mavrikakis, *Surf. Sci.* **587**, 159 (2005).
- <sup>15</sup>H. Tang and B. L. Trout, *J. Phys. Chem. B* **109**, 17630 (2005).
- <sup>16</sup>M. Gajdoš, J. Hafner, and A. Eichler, *J. Phys.: Condens. Matter* **18**, 13 (2006).
- <sup>17</sup>R. B. Getman and W. F. Schneider, *J. Phys. Chem. C* **111**, 389 (2007).
- <sup>18</sup>J. G. Wang *et al.*, *Phys. Rev. Lett.* **95**, 256102 (2005).
- <sup>19</sup>A. Beutler, E. Lundgren, R. Nyholm, J. N. Andersen, B. J. Setlik, and D. Heskett, *Surf. Sci.* **396**, 117 (1998).
- <sup>20</sup>M. Smedh, A. Beutler, T. Ramsvik, R. Nyholm, M. Borg, J. N. Andersen, R. Duschek, M. Sock, F. P. Netzer, and M. G. Ramsey, *Surf. Sci.* **491**, 99 (2001).
- <sup>21</sup>A. Baraldi, G. Comelli, S. Lizzit, M. Kiskinova, and G. Paolucci, *Surf. Sci. Rep.* **49**, 169 (2003).
- <sup>22</sup>M. Birgersson, C. O. Almbladh, M. Borg, and J. N. Andersen, *Phys. Rev. B* **67**, 045402 (2003).
- <sup>23</sup>L. Köhler and G. Kresse, *Phys. Rev. B* **70**, 165405 (2004).
- <sup>24</sup>W. Ji, Z.-Y. Lu, and H. Gao, *Phys. Rev. Lett.* **97**, 246101 (2006).
- <sup>25</sup>W. Zhang, J. Yang, Y. Luo, S. Monti, and V. Carravetta, *J. Chem. Phys.* **129**, 064703 (2008).
- <sup>26</sup>P. Hohenberg and W. Kohn, *Phys. Rev.* **136**, B864 (1964).
- <sup>27</sup>W. Kohn and L. J. Sham, *Phys. Rev.* **140**, A1133 (1965).
- <sup>28</sup>J. P. Perdew, K. Burke, and M. Ernzerhof, *Phys. Rev. Lett.* **77**, 3865 (1996).
- <sup>29</sup>D. Vanderbilt, *Phys. Rev. B* **41**, 7892 (1990).
- <sup>30</sup>B. Hammer, L. B. Hansen, and J. K. Nørskov, *Phys. Rev. B* **59**, 7413 (1999).
- <sup>31</sup>P. E. Blöchl, *Phys. Rev. B* **50**, 17953 (1994).
- <sup>32</sup>G. Kresse and D. Joubert, *Phys. Rev. B* **59**, 1758 (1999).
- <sup>33</sup>M. Marsman and G. Kresse, *J. Chem. Phys.* **125**, 104101 (2006).
- <sup>34</sup>G. Kresse and J. Furthmüller, *Phys. Rev. B* **54**, 11169 (1996).
- <sup>35</sup>H. J. Monkhorst and J. D. Pack, *Phys. Rev. B* **13**, 5188 (1976).
- <sup>36</sup>C. Kittel, *Introduction to Solid State Physics*, 7th ed. (Wiley, New York, 1996).
- <sup>37</sup>A. Zupan, P. Blaha, K. Schwarz, and J. P. Perdew, *Phys. Rev. B* **58**, 11266 (1998).
- <sup>38</sup>M. Fuchs, J. L. F. Da Silva, C. Stampfl, J. Neugebauer, and M. Scheffler, *Phys. Rev. B* **65**, 245212 (2002).
- <sup>39</sup>J. L. F. Da Silva, C. Stampfl, and M. Scheffler, *Surf. Sci.* **600**, 703 (2006).
- <sup>40</sup>H. Jónsson, G. Mills, and K. W. Jacobsen, *Classical and Quantum Dynamics in Condensed Phase Simulations* (World Scientific, Singapore, 1998).
- <sup>41</sup>G. Henkelman, B. P. Uberuaga, and H. Jónsson, *J. Chem. Phys.* **113**, 9901 (2000).
- <sup>42</sup>G. Henkelman and H. Jónsson, *J. Chem. Phys.* **113**, 9978 (2000).
- <sup>43</sup>E. L. Jeffery, R. K. Mann, G. J. Hutchings, S. H. Taylor, and D. J. Willock, *Catal. Today* **105**, 85 (2005).
- <sup>44</sup>D. L. Adams, H. B. Nielsen, and M. A. Van Hove, *Phys. Rev. B* **20**, 4789 (1979).
- <sup>45</sup>W. K. Offermans, A. P. J. Jansen, and R. A. van Santen, *Surf. Sci.* **600**, 1714 (2006).
- <sup>46</sup>J. E. Demuth, *Chem. Phys. Lett.* **45**, 12 (1977).
- <sup>47</sup>G. B. Fisher, *Chem. Phys. Lett.* **79**, 452 (1981).
- <sup>48</sup>G. N. Derry and Zhang Ji-Zhong, *Phys. Rev. B* **39**, 1940 (1989).
- <sup>49</sup>Computational chemistry comparison and benchmark database (cccbdb) <http://cccbdb.nist.gov>
- <sup>50</sup>C. Adamo and V. Barone, *J. Chem. Phys.* **110**, 6158 (1999).
- <sup>51</sup>J. Paier, R. Hirschl, M. Marsman, and G. Kresse, *J. Chem. Phys.* **122**, 234102 (2005).
- <sup>52</sup>J. Paier, M. Marsman, K. Hummer, G. Kresse, I. C. Gerber, and J. G. Ángyán, *J. Chem. Phys.* **124**, 154709 (2006).
- <sup>53</sup>J. L. F. Da Silva, M. V. Ganduglia-Pirovano, J. Sauer, V. Bayer, and G. Kresse, *Phys. Rev. B* **75**, 045121 (2007).
- <sup>54</sup>G. S. Karlberg, T. F. Jaramillo, E. Skúlason, J. Rossmeisl, T. Bligaard, and J. K. Nørskov, *Phys. Rev. Lett.* **99**, 126101 (2007).
- <sup>55</sup>H.-Y. Su, M.-M. Yang, X.-H. Bao, and W.-X. Li, *J. Phys. Chem. C* **112**, 17303 (2008).
- <sup>56</sup>P. J. Feibelman, B. Hammer, J. K. Nørskov, F. Wagner, M. Scheffler, R. Stumpf, R. Watwe, and J. Dumesic, *J. Phys. Chem. B* **105**, 4018 (2001).
- <sup>57</sup>C. E. Wartnaby, A. Stuck, Y. Y. Yee, and D. A. King, *J. Phys. Chem.* **100**, 12483 (1996).
- <sup>58</sup>K. H. Hansen, Z. Sljivancanin, B. Hammer, E. Laegsgaard, F. Besenbacher, and I. Stensgaard, *Surf. Sci.* **496**, 1 (2002).
- <sup>59</sup>J. L. Gland and B. A. Sexton, *Surf. Sci.* **94**, 355 (1980).
- <sup>60</sup>B. E. Hayden, *Surf. Sci.* **131**, 419 (1983).
- <sup>61</sup>V. K. Agrawal and M. Trenary, *Surf. Sci.* **259**, 116 (1991).
- <sup>62</sup>J. Yoshinobu and M. Kawai, *Chem. Lett.* **24**, 605 (1995).
- <sup>63</sup>A. L. Allred, *J. Inorg. Nucl. Chem.* **17**, 215 (1961).
- <sup>64</sup>J. L. F. Da Silva and C. Stampfl, *Phys. Rev. B* **76**, 085301 (2007).
- <sup>65</sup>A. Michaelides, P. Hu, M. H. Lee, A. Alavi, and D. A. King, *Phys. Rev. Lett.* **90**, 246103 (2003).
- <sup>66</sup>L. D. Schmidt and R. Gomer, *J. Chem. Phys.* **45**, 1605 (1966).
- <sup>67</sup>W. X. Li, C. Stampfl, and M. Scheffler, *Phys. Rev. B* **65**, 075407 (2002).
- <sup>68</sup>Y. Wang, S. de Gironcoli, N. S. Hush, and J. R. Reimers, *J. Am. Chem. Soc.* **129**, 10402 (2007).
- <sup>69</sup>K. Doll, *Surf. Sci.* **573**, 464 (2004).

- <sup>70</sup>S. E. Mason, I. Grinberg, and A. M. Rappe, *Phys. Rev. B* **69**, 161401(R) (2004).
- <sup>71</sup>G. Kresse, A. Gil, and P. Sautet, *Phys. Rev. B* **68**, 073401 (2003).
- <sup>72</sup>A. Gil, A. Clotet, J. M. Ricart, G. Kresse, M. Garcia-Hernandez, N. Rosch, and P. Sautet, *Surf. Sci.* **530**, 71 (2003).
- <sup>73</sup>Q. M. Hu, K. Reuter, and M. Scheffler, *Phys. Rev. Lett.* **98**, 176103 (2007).
- <sup>74</sup>M. Neef and K. Doll, *Surf. Sci.* **600**, 1085 (2006).
- <sup>75</sup>M. Gajdoš and J. Hafner, *Surf. Sci.* **590**, 117 (2005).
- <sup>76</sup>M. Alaei, H. Akbarzadeh, H. Gholizadeh, and S. de Gironcoli, *Phys. Rev. B* **77**, 085414 (2008).
- <sup>77</sup>S. Hüfner, *Photoelectron Spectroscopy: Principles and Applications*, 3rd ed. (Springer-Verlag, Berlin, 2003).
- <sup>78</sup>L. Bianchettin, A. Baraldi, S. de Gironcoli, E. Vesselli, S. Lizzit, L. Petaccia, G. Comelli, and R. Rosei, *J. Chem. Phys.* **128**, 114706 (2008).
- <sup>79</sup>E. Vesselli, M. Campaniello, A. Baraldi, L. Bianchettin, C. Africh, F. Esch, S. Lizzit, and G. Comelli, *J. Phys. Chem. C* **112**, 14475 (2008).
- <sup>80</sup>P. Finn, R. K. Pearson, J. M. Hollander, and W. L. Jolly, *Inorg. Chem.* **10**, 378 (1971).